



Retinal image segmentation using double-scale non-linear thresholding on vessel support regions

ISSN 2468-2322

Received on 10th May 2017

Revised on 6th June 2017

Accepted on 15th June 2017

doi: 10.1049/trit.2017.0013

www.ietdl.org

Qingyong Li¹ ✉, Min Zheng¹, Feng Li¹, Jianzhu Wang¹, Yangli-ao Geng¹, Haibo Jiang²

¹Beijing Key Lab of Transportation Data Analysis and Mining, Beijing Jiaotong University, Beijing 100044, People's Republic of China

²Department of Ophthalmology, Xiangya Hospital, Central South University, Changsha 410083, People's Republic of China

✉ E-mail: liqy@bjtu.edu.cn

Abstract: Retinal vessel segmentation is a critical indicator of diagnosis, screening, and treatment of cardiovascular and ophthalmologic diseases. Due to the fact that the retinal vessels usually have some tiny structures and blurred boundaries, especially with remarkable noises, it is difficult to correctly segment the vascular networks. In this study, the authors propose a double-scale non-linear thresholding method based on vessel support regions. First, the double-scale filtering method is applied to enhance the contrast between the foreground vascular and the background stuffs. Second, they segment the fine and coarse vessels by the corresponding adaptive local thresholding and fixed-ratio thresholding method. Finally, they obtain the binary segmentation by fusion of fine and coarse vessels. Experiments are conducted on the publicly available DRIVE and STARE datasets, which show the effectiveness of the proposed method on retinal vessel segmentation.

1 Introduction

Accurate detection and analysis of retinal blood vessels have been widely used for diagnosis, screening, and treatment of cardiovascular and ophthalmologic diseases, including diabetic retinopathy, hypertension, and arteriosclerosis [1–5]. Due to the inhomogeneous distribution of the grey-level profiles, the complicated structure of the vessels, the poor local contrast between foreground objects and background stuff, and the image noise from the acquisition, it is difficult to segment vessels from retinal images. In the past few decades, several methods have been proposed for the segmentation of vessels in retinal images. In general, they can be divided into two methods: supervised and unsupervised methods. The supervised methods require some prior labelling information to decide whether a pixel belongs to a vessel or not [6–11], whereas the unsupervised methods do the vessel segmentation without any prior labelling knowledge.

1.1 Supervised method

The supervised methods usually utilise ground truth data for the classification of vessels which is based on given features. In essence, this method exploits a set of manually labelled rules of vessel extraction on the basis of a training set to discriminate whether a pixel belongs to a vessel or not. Undoubtedly, feature extraction and classifier determine the performance of the methods. For example, Staal *et al.* conducted the feature vector extracted from image ridges and a K-nearest neighbours (KNN) classifier [6]. In [8], Ricci and Perfetti used line operators and support vector machine classification with three features per pixel. In [9], Marin *et al.* used a neural network (NN) scheme for pixel classification and computed a seven-dimensional (7D) vector composed of grey-level and moment invariant-based features for pixel representation. In [10], Fraz *et al.* introduced an AdaBoost classifier for vessel segmentation which utilises a 9D feature vector extracted from the green plan of the red-, green-, and blue-coloured images without any pre-processing. In [11], Cheng *et al.* introduced a feature-based AdaBoost classifier for vessel segmentation which utilises a 41D feature vector at different spatial scales for each pixel. In [4], Li *et al.* applied a deep NN to model the vessel map

and achieved an effective result. In general, supervised methods exhibit effective and efficient performance in segmentation. However, the vessel segmentation based on the classifier still has difficulty in the clinic, since those massive retinal images, which have been segmented completely, are inevitable as the criterial ground truth.

1.2 Unsupervised method

Unsupervised methods, also known as the rule-based methods, can be further classified into matched filtering, vessel tracking, morphological processing, and partial adaptive threshold approaches.

Among the various retinal vessel segmentation methods, the classical-matched filtering method is a widely simple yet effective one. The concept of the matched filter, first presented by Chaudhuri *et al.* [12], was detected by the piecewise linear segmentation of blood vessels in the retinal images. This technique convolved a 2D kernel with the retinal image and extracted 12 different templates that were used to search for vessel segments along all possible directions. In [13], Hoover *et al.* proposed a piecewise thresholding algorithm based on matched filter response and proved that retinal vessels are iteratively decreasing with piecewise thresholds. Later, the matched filtering method has been enhanced from abundant scopes [14, 15].

The vessel tracking method is a representative method in unsupervised methods. For example, in [16], Zou *et al.* presented a method based on analysing the consecutive scanlines. The consecutive scanline-fitting strategy gives accurate vessel direction estimates and further, these directions can be used in vessel tracking. Recently, Yin *et al.* [17] proposed a technique based on the probabilistic tracking method. During the tracking process, vessel edge points are detected iteratively using local grey-level statistics and continuity properties of vessels.

The morphological processing method has been universally used in the vessel segmentation, as the retinal vessels have obvious morphological characteristics such as linearity and inflection. In [18], Mendonca and Campilho proposed an automated method for the segmentation of the vascular networks in retinal images. This method proposed herein can be described in three main processing phases. First, a top-hat transform with variable size structuring

elements is aimed at enhancing the vessels with different widths. Second, in order to obtain the initial vascular network, the morphological reconstruction method is applied. Finally, the final segmentation is carried out by combining the extracted centrelines. Additionally, in [19], the traditional retinal blood vessel segmentation method had been improved. The proposed method is based on the linear combination of line detectors at varying scales, which avoids the issues caused by each individual line detector. Nevertheless, to some degree, there are some errors in the extraction of the retinal blood vessels. Moreover, in [20], first, for noise removal and vessel localisation, the authors applied a multi-scale hierarchical decomposition, which is extremely effective for the normalised enhanced images. Then, a binary map of vasculature was obtained by an adaptive local thresholding (ALT) method. This method can effectively estimate the noise and has a high segmentation precision for the retinal lesion images.

The partial adaptive thresholds method is also a well-known unsupervised method. For example, in [21], Jiang and Mojon proposed a general framework of ALT using a verification-based multi-threshold probing scheme. This approach is regarded as knowledge-guided adaptive thresholding, in contrast to most of the algorithms known from the literature.

Aiming to address these challenges of retinal vessel segmentation, we present the double-scale non-linear thresholding (DNT) algorithm, which is based on the vessel support regions (VSRs). The segmentation task is remoulded as a cross-modality problem. The first modality is the fine vessel segmentation (FVS), while the second modality is the coarse vessel segmentation (CVS). Furthermore, the final segmentation result is obtained by fusion of fine and coarse (FFC) vessels. The main contributions of this study include the following:

- (i) The authors propose a novel double-scale filtering (DSF) method to improve the contrast of fine and coarse vessels, respectively.
- (ii) For fine vessels, we utilise a new ALT method on VSRs to achieve the binary segmentation of vessels.
- (iii) For coarse vessels, we present a fixed-ratio thresholding (FRT) method to tackle segmentation.

This paper is organised as follows. Section 2 briefly describes the overview of the proposed DNT method. The proposed method is presented in Section 3. In Section 4, the performance metrics of the algorithm are assessed by experiments. Finally, discussion and conclusion are given in Section 5.

2 Overview

In this study, we propose a novel method, namely DNT. It has been schematically described in Fig. 1, where the core segmentation algorithm consists of three main stages.

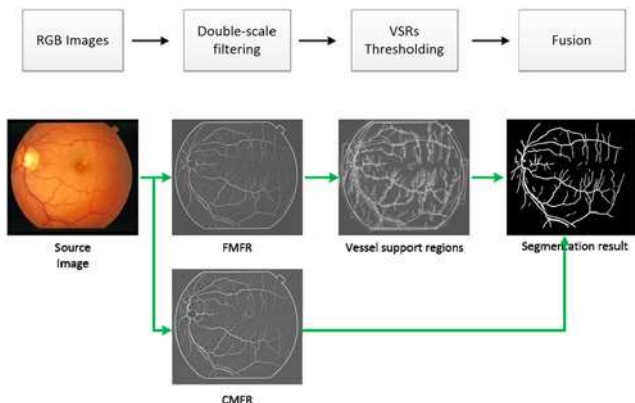


Fig. 1 Overview of the proposed VSR method

2.1 Double-scale filtering (DSF)

Blood vessels have poor local contrast and universally the Gaussian-matched filter is used to improve the contrast between the vessels and the background. The Gaussian-matched filter in different scales has corresponding enhancement effects on fine and coarse vessels, respectively. Accordingly, to be more specific, to complete the tasks of fine-matched filtering response (FMFR) and coarse-matched filtering response (CMFR), we need to design two kinds of Gaussian functions, i.e. fine-scale Gaussian function and coarse-scale Gaussian function, which are separately convolved with the green channel of the retinal image.

2.2 Adaptive local thresholding (ALT)

The Gaussian-matched filter has enhanced the contrast of the FMFR image, and meanwhile, the regions of macular and lesions have been inhibited. However, there still exists the nuisance that the distribution of grey in FMFR images is inhomogeneous, and considerable greys between the foreground and the background are difficult to be distinguished. Theoretically, it is impossible to discover a global threshold that can achieve the task of linear segmentation between the blood vessels and the background. VSR refers to a rectangle that contains a vessel segment, which can be automatically detected by algorithms. Usually, the scales of VSRs are not identical. For the large-scale VSRs, by virtue of their bi-modal histograms, segmentation between the vessels and the background stuffs is achieved by Otsu algorithm [22]. In contrast, for the small-scale VSRs, due to their unimodal histograms, we use Swt algorithm [23] to segment vessels. ALT phase contains three main steps: first, all VSRs in FMFR images are automatically detected by the VSR detector. Second, we proposed a combination of Otsu and Swt (COS) method, which achieves the corresponding binarisation of large and small VSRs by Otsu and Swt, respectively. Finally, we conduct the binary segmentation by fusion of the fine and coarse vessels. Also, at the same time, all pixels that do not belong to the VSRs are set as the background. In this way, FVS is obtained.

2.3 FFC vessels

This phase consists of two stages: first, in order to obtain the CVS, we utilise an FRT method to segment the CMFR image. Second, by the logic or operator, the FVS and CVS are fused into a single binary image, which contains the fine vessels and coarse vessels simultaneously.

3 Double-scale non-linear thresholding (DNT)

The DNT consists of three main phases: DSF, ALT, and FFC. These steps are described as the following.

3.1 Double-scale filtering (DSF)

The retinal colourful image contains three plans – red, green, blue. In which the green channel exhibits the best contrast between the vessels and background while the red and blue ones tend to be noisier. Thus, we always prefer the green channel for further process in vessel segmentation compared with the other two plans.

In retinal vessel images, the centre pixels appear darker relative to their neighbourhood. Blood vessel grey-level profile can be approximated by a Gaussian-shaped curve. The Gaussian-matched filter, therefore, is generally used for enhancing the contrast of retinal images.

Now let us suppose that the vessels are considered as piecewise linear segments. For our initial calculations, we shall assume that all of the blood vessels in the image are of equal width 2δ and of length L . Consequently, a Gaussian function is proposed as a model for the grey-level profile of the cross-section of the vessels.

Also, such a kernel may be mathematically expressed as

$$K(x, y) = \exp\left(-\frac{x^2}{2\delta^2}\right), \quad |x| \leq 3\delta, \quad |y| \leq \frac{L}{2}, \quad (1)$$

where $K(x, y)$ is the kernel function, δ represents the scale of the filter, and L is the length of the segment for which the vessel is assumed to have a fixed orientation. Here the direction of the vessel is assumed to be aligned along the y -axis. In our implementation, $L = 5$.

Given the arbitrary directions of the blood vessels, we first construct 12 different templates that are used to search for vessel segments along all possible directions. Then, a set of 12 such templates are applied to a fundus image and only the maximum of their responses is retained at each pixel. In order to facilitate the sub-processing, the matched filtering response image is usually normalised and quantified as the 256 grey-level scales.

Usually, retinal vessel images consist of fine and coarse vessels simultaneously. We observe that fine-matched filter (FMF) is adapted to respond to fine vessels and erode coarse vessels. Conversely, coarse-matched filter (CMF) is adapted to segment coarse vessels and blur fine vessels. Fig. 2 illustrates the corresponding matched filter images for different values of δ .

In this step, we look for a DSF for pre-processing. For fine vessels, we apply FMF to segment fine vessels. For coarse vessel, we apply CMF to respond to the coarse vessels.

3.2 ALT on VSRs

The ALT method finds an optimal threshold for each local region and non-linearly segments FMFR images, in order to overcome the linearly non-separable problem faced by global thresholding methods. This section presents a new ALT algorithm, which is based on VSRs, known as Otsu thresholding method and Swt algorithm. ALT first detects the VSRs in the gradient space of FMFR images using a vessel segment detector and then the authors present a COS method to achieve the corresponding binarisation of large and small VSRs. Finally, the small and large VSRs are fused into one binary image.

3.2.1 VSR detection: A VSR denotes a locally straight vessel segment in a retinal image. Generally, a VSR contains a line contour where the grey level is notably changing from dark to light or the opposite. The gradient of FMFR images, therefore, is

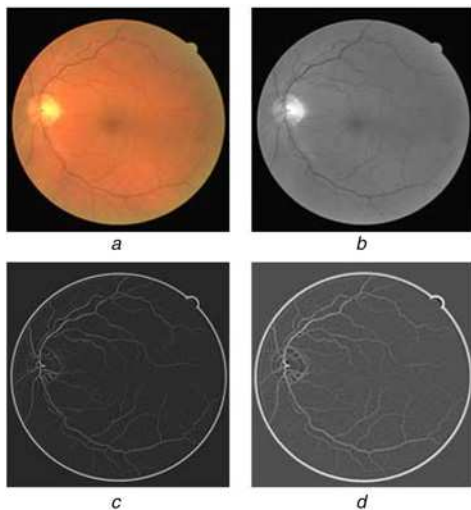


Fig. 2 Pre-processing of retinal images

- a Example of colour image
- b Grey image of green channel
- c FMFR image with $\delta = 1.3$ and $L = 5$
- d CMFR image with $\delta = 2.3$ and $L = 5$

applied for detecting VSRs, as gradients represent such grey change. The VSR detector starts by computing the gradient of each pixel at an FMFR image. The image is then segmented into connected regions of pixels that share the same gradient angle up to tolerance τ . Such connected regions are denoted as VSRs. Each VSR is a candidate of a straight vessel segment and is associated with a rectangle.

The VSR detector takes an FMFR image as input and returns a list of rectangles that include a vessel segment. This algorithm includes three main steps, i.e. gradient computing and filtering, region growing, and rectangle extension. Algorithm 1 (see Fig. 3) presents a complete description in pseudo-code.

(i) *Gradient computing and filtering:* Given an FMFR image M and a pixel P at a coordinate (x, y) , its gradient is computed as follows:

$$g_X(x, y) = \frac{M(x+1, y) + M(x+1, y+1) - M(x, y) - M(x, y+1)}{2}, \quad (2)$$

$$g_Y(x, y) = \frac{M(x, y+1) + M(x+1, y+1) - M(x, y) - M(x+1, y)}{2}, \quad (3)$$

where $M(x, y)$ refers to the grey value of the pixel $P(x, y)$. The gradient angle is calculated as

$$A(x, y) = \arctan\left(\frac{g_X(x, y)}{-g_Y(x, y)}\right) \quad (4)$$

and the gradient magnitude is computed as

$$G(x, y) = \sqrt{g_X^2(x, y) + g_Y^2(x, y)}. \quad (5)$$

Generally, pixels with high gradient magnitude correspond to the edges or noises. In a vessel segment, the edge pixels usually have the highest gradient magnitude, so it is a good choice to set such pixels as seed points to search vessel segment.

A bucket sorting algorithm is applied to obtain a descending bin sequence, and each bin contains pixels with a similar gradient magnitude. The VSR detector first uses the pixels in the largest bin as seed pixels, and then it takes seed pixels from the second bin, and so on until it uses up all considered bins.

We observe that pixels with small gradient magnitude often correspond to the background and they should not be treated as seed pixels. In addition, the proportion of vessel pixels in a retinal image is far lower than that of background. For example, the average proportion of vessel pixels in DRIVE and STAREs datasets is 8.43 and 7.60%, respectively. So the descending bin sequence is truncated by a threshold ρ , which makes about the top 10% proportion of pixels to be considered as seed points. Our

Input: A FMFR image M
Output: A list V of rectangles

- 1 $(A, G) \leftarrow \text{Gradient}(I)$;
- 2 (Descending pixel list L, ρ) $\leftarrow \text{GradientFilter}(I)$
- 3

$$S \leftarrow \begin{cases} \text{USED, pixels with } M \leq \rho \\ \text{UNUSED, otherwise} \end{cases}$$

For each pixel $P \in L$ do

- 4 if $S(P) = \text{UNUSED}$ then
 - connected region $C \leftarrow \text{RegionGrow}(P, \tau)$;
 - vessel support region $V \leftarrow \text{RectExtend}(C)$;
- end

Fig. 3 Algorithm 1: VSRs detector

experiments verify that such a truncation strategy can notably improve the computing efficiency and does not degrade segmentation performance.

(ii) *Region growing*: A region growing algorithm is applied to form a VSR starting from an unused seed pixel. Note that the status of all pixels, whose gradient magnitude is $> \rho$, is set to UNUSED and the other pixels are set to USED. The status is saved in an auxiliary matrix \mathcal{S} , which has the same size as the FMFR image \mathcal{M} . First, a seed pixel P is selected and a region C is created whose angle A_C is initialised with $A(P)$. Recursively, all unused neighbours of the pixels included in C are checked, and the neighbours whose gradient angle is equal to A_C up to tolerance τ are included in C . Note that an eight-connected neighbourhood is used. When a pixel is added to C , the region angle value is updated to

$$A_C = \arctan\left(\frac{\sum_k \sin(A(k))}{\sum_k \cos(A(k))}\right), \quad (6)$$

where k refers to the index of pixels added to C . This process is repeated until no other pixel can be added to C .

(iii) *Rectangle extension*: After the region growing algorithm collects a set of pixels with similar gradient angles, the rectangle R associated with C will be computed and extended. The centre O of the rectangle is set to the centre of the mass of C and the main direction of R is set to the first inertia axis of C , as applied in [23]. In addition, the width ω and length h of R are set to the smallest

values that make the rectangle to cover the full connected region C . In other words, R is the minimum circumscribed rectangle of C .

The circumscribed R can cover most edge pixels of a vessel segment, but it needs to be extended because of two factors. First, a vessel segment can usually be divided into two connected regions because of the gradient directions of the pixels at the different side of the vessel are opposite. Second, some intersections of vessels are neglected because of the irregularity in their gradient magnitude or angle. Fig. 4a shows some examples of such rectangles.

The rectangle R extends $\omega/2$ pixels from both the first and the second inertia axes and produces a vessel support region V as demonstrated in Figs. 4b and c. This procedure is simple but effective to cover all pixels of a vessel segment. Note that the pixels in the extended region are marked as USED, as they are included in a VSR.

3.2.2 VSR binarisation: A set of VSRs in an FMFR image is detected by the above-mentioned VSR detection method. We observe that the VSR, whose scale is $> 2s$, appears as a bi-modal histogram. The VSR, whose scale is $< 2s$, appears as a unimodal histogram. Fig. 5 shows the grey histogram of VSRs. In this step, we proposed a COS method to achieve the corresponding binarisation of large and small VSRs. For the large-scale VSRs, the segmentation of the vessels from the background is achieved by the Otsu algorithm and for the small-scale VSRs, we utilise the Swt algorithm to segment the vessels. Subsequently, the small and large VSRs are fused into one binary image. The process of VSR binarisation is shown in Fig. 6.

3.3 FFC vessels

Fine vessels can be segmented by the ALT algorithm. Unfortunately, for coarse vessels, ALT can only segment their rough skeleton and still miss some pixels. In our method, first, we present a novel FRT method to segment the CMFR image, and then the CVS is obtained. Second, we use the operator of *logic* to fuse the FVS and CVS into one single binary image, which consists of the fine vessels and coarse vessels simultaneously. FFC vessels are shown in Fig. 7.

The FRT method consists of three steps: first, sort the pixels of the CMF image in descending order by the bucket order algorithm;

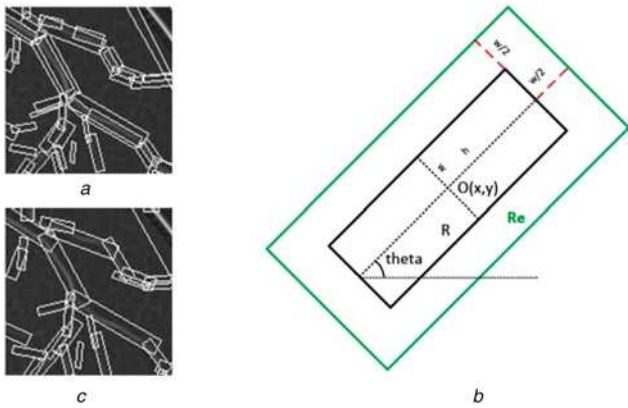


Fig. 4 Illustration of rectangle extension

a Rectangle obtained by region growing algorithm
b Rectangle extension on both the first and the second inertia axes
c Extended rectangle

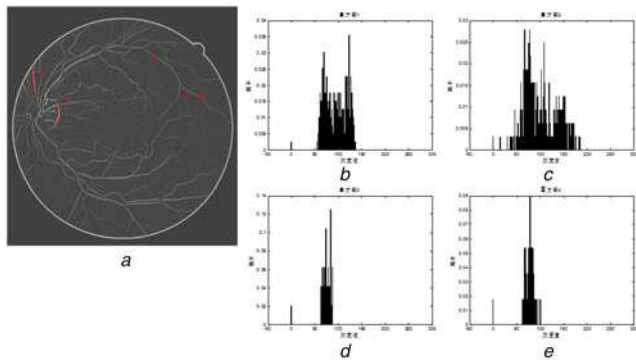


Fig. 5 Grey histogram of VSRs

a MFR image and four randomly selected VSRs that are marked with red rectangle
b Histogram of VSR1
c Histogram of VSR2
d Histogram of VSR3
e Histogram of VSR4

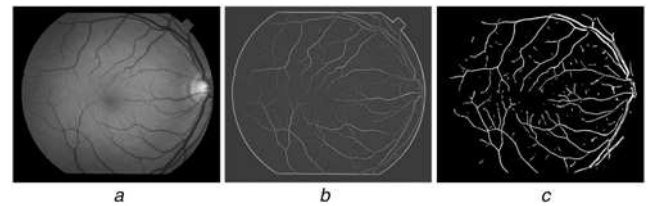


Fig. 6 The process of VSR binarisation

a Green channel of the retinal image
b FMFR image
c Segmentation result of VSR binarisation

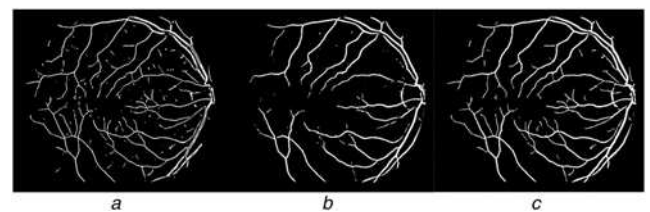


Fig. 7 FFC vessels

a Segmentation result of ALT-VSR
b Segmentation result of FRT
c Final segmentation result

second, calculate the optimal threshold T_r ; third, binarise the CMF image according to T_r . Directly, the retinal images have the obvious distinction of distribution between the linear vascular and the background stuff. Also, the ratio of the foreground is usually lower than the background. In this method, the threshold T_r is given by

$$T_r = \text{Min} \left(\frac{\text{Num}(M(x, y) \geq t)}{\text{Total}} \leq t \right), \quad (7)$$

where r represents the expected ratio of the vascular, Total is the quantity of all pixels, and Num is the frequency function. FRT has binary outputs. Fig. 7b shows the segmentation result of FRT.

4 Experimental results and analysis

In this section, we evaluate and compare the performance of our algorithm against previous algorithms on two representative benchmark datasets: the DRIVE dataset and the STARE dataset.

4.1 Experimental setup

4.1.1 Datasets: The DRIVE dataset [6] contains a total of 40 colour retinal images, which are divided into a training set and a test set, both containing 20 images. Each image was captured at 565×584 pixels. For each image in DRIVE, the manually segmented vessel tree is provided along with a binary mask for the field of view (FOV) area.

The STARE dataset [13] contains 20 retinal images, in which ten of them are from the healthy ocular fundus and the other ten images are from unhealthy ones. Each image was sized to 700×605 pixels.

Two manual segmentations, which were made by two independent human observers, are available for each image of the three datasets. The manually segmented images by the first human observer are used as a ground truth as used in [4, 10], and the human observer performance is measured using the manual segmentations by the second human observer. The binary mask for the FOV for each image in DRIVE is available, and the FOV binary masks for STARE and CHASE are manually created as described in [7].

4.1.2 Evaluation criterion: Vessel segmentation can be regarded as a binary classification problem, and there are two class labels for each pixel of a retinal image: vessel and non-vessel. Comparing the automatically segmented results with the manually ground truth, we can observe four types of results: true positives (TPs) refer to the vessel pixels that are predicted as vessels, false negatives (FNs) refer to the vessel pixels that are predicted as non-vessels, true negatives (TNs) refer to the non-vessel pixels that are predicted as non-vessels, and false positives (FPs) denote the non-vessel pixels that are predicted as vessels.

We use four criteria to compare the performance of the proposed method with other state-of-the-art methods, i.e. the sensitivity (Se), specificity (Sp), accuracy (Acc) and F -measure (F). These measures are computed as

$$\text{Se} = \frac{\text{TP}}{\text{TP} + \text{FN}}, \quad (8)$$

$$\text{Sp} = \frac{\text{TN}}{\text{TN} + \text{FP}}, \quad (9)$$

$$\text{Acc} = \frac{\text{TP} + \text{TN}}{\text{TP} + \text{FN} + \text{TN} + \text{FP}}, \quad (10)$$

$$F = 2 \times \frac{P_r \times S_e}{P_r + S_e}, \quad (11)$$

where P_r is defined as $\text{TP}/(\text{TP} + \text{FP})$.

Table 1 DSF performance compared with FMF and CMF methods on DRIVE and STARE datasets

Dataset	Method	Se	Sp	Acc	F -measure
DRIVE	FMF	0.4851	0.9900	0.9254	9.6221
	CMF	0.6531	0.9806	0.9386	0.7290
	DSF	0.6924	0.9783	0.9416	0.7500
STARE	FMF	0.5444	0.9835	0.9389	0.6377
	CMF	0.6074	0.9830	0.9434	0.6855
	DSF	0.7126	0.9746	0.9474	0.7332

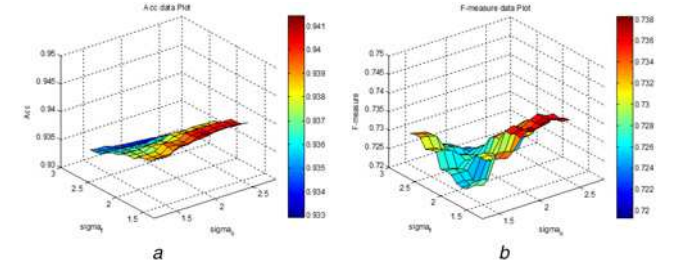


Fig. 8 Segmentation performance of DNT as a function of δ_f and δ_c on DRIVE dataset

a Result of Acc
b Result of F -measure

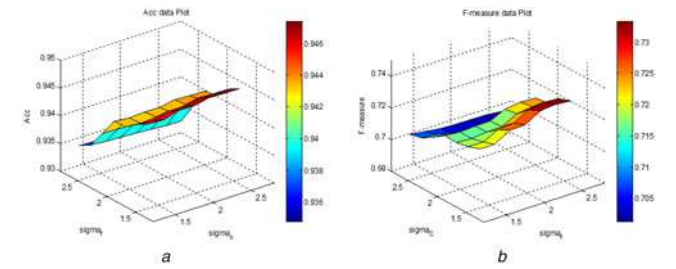


Fig. 9 Segmentation performance of DNT as a function of δ_f and δ_c on STARE dataset

a Result of Acc
b Result of F -measure

Table 2 COS performance compared with Otsu and CMF methods on DRIVE and STARE datasets

Dataset	Method	Se	Sp	Acc	F -measure
DRIVE	COS	0.6924	0.9783	0.9416	0.7500
	Otsu	0.6819	0.9794	0.9412	0.7460
	Swf	0.7010	0.9719	0.9371	0.7383
STARE	COS	0.7126	0.9746	0.9475	0.7332
	Otsu	0.6725	0.9793	0.9473	0.7208
	Swf	0.7314	0.9675	0.9427	0.7232

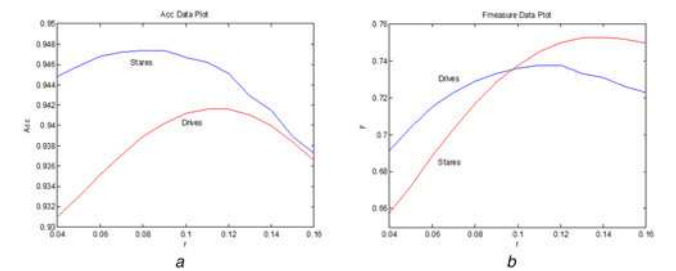


Fig. 10 Segmentation performance of DNT as a function of r

a Result of Acc
b Result of F -Measure

4.2 Evaluation metric

In our experiment, a DSF is applied for pre-processing. Table 1 summarises the result of the proposed DSF method in comparison with the uniscale thresholding method, i.e. FMF and CMF on both DRIVE and STARE datasets. From this table, we observe that

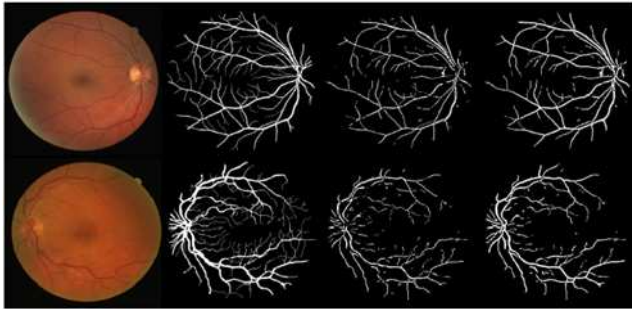


Fig. 11 Segmentation results for the DRIVE dataset. The first four columns are the retinal images, manual segmentation, ALT segmentation, and DNT segmentation. The first row has the best accuracy, and the second row has the worst accuracy

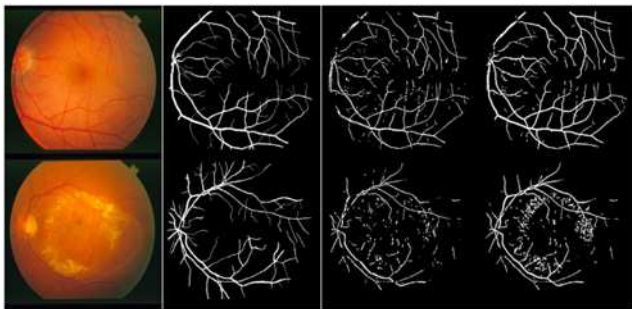


Fig. 12 Segmentation results for the STARE dataset. The first through fourth columns are the retinal images, manual segmentation, ALT segmentation, and DNT segmentation. The first row is the best accuracy, and the second row has the worst accuracy

our DSF algorithm has excellent pre-processing performance. The proposed DSF method achieves better performance than the uniscale thresholding methods regarding the Se, Sp, Acc, and F jointly.

The effectiveness of the proposed DSF strategy is validated through experiments on two public benchmark datasets above. Consequently, we should conduct an optimal threshold δ of DSF to improve the contrast between the vessels and the background.

For fine-scale Gaussian function and coarse-scale Gaussian function, we assume that $\delta = \delta_f$ and $\delta = \delta_c$, respectively, where δ represents the scale of Gaussian-matched filter. The segmentation performances of DNT as a function of δ_f and δ_c on DRIVE and STARE datasets are, respectively, shown in Figs. 8 and 9. We can observe that Acc and F increase first and then decrease along with the rising of δ_c when δ_f is fixed. Acc and F reach the maximum while $\delta_c = 2.3$. Similarly, fixing δ_c , when $\delta_f = 2.3$, Acc and F get the peak. Therefore, in our experiment, we set $\delta_c = 2.3$ and $\delta_f = 1.3$.

In addition, in the ALT phase, we utilise a novel COS algorithm to achieve the processing of VSR binarisation. COS values are higher than those of single methods: Otsu or Swt methods. The results of the proposed COS method are compared with those of the previous Otsu or Swt methods in Table 2 for the DRIVE and STARE datasets.

For the coarse vessels, in our experiment, we apply the FRT method to the segment. Fig. 10 shows the segmentation performance of DNT as a function of r . Obviously, both Acc and F increase first and then decrease with the increasing of r . On the DRIVE dataset, when $r=0.12$, Acc reaches the peak. On the STARE dataset, when $r=0.12$, Acc reaches the peak. Similarly, F also presents this trend.

Figs. 11 and 12 show the final segmentation results for the DRIVE and STARE dataset.

4.3 Comparison with the state-of-the-art

Tables 3 and 4 list the qualitative evaluation of our approach along with the results reported in previous studies for DRIVE and STARE datasets. From these tables, we see that compared with unsupervised methods, the proposed method produces greater results and outperforms previous state-of-the-art unsupervised solutions. On comparison with supervised methods, our algorithm does not require a set of manually labelled rules of

Table 3 Performance comparison with the state-of-the-art methods on the DRIVE dataset

Type	Methods	Year	Se	Sp	Acc	F -measure
supervised methods	Staal <i>et al.</i> [6]	2004	N.A	N.A	0.9442	N.A
	Li <i>et al.</i> [4]	2016	0.7569	0.9816	0.9527	N.A
unsupervised methods	Jiang and Mojon [21]	2003	N.A	N.A	0.9212	N.A
	Martinez-Perez <i>et al.</i> [24]	2007	N.A	N.A	0.9344	N.A
	Yin <i>et al.</i> [17]	2012	0.7154	0.9716	0.9267	N.A
	Li <i>et al.</i> [15]	2012	0.7154	0.9716	0.9343	N.A
	Wang <i>et al.</i> [25]	2015	0.7527	0.9744	0.9457	N.A
	proposed method	2017	0.6924	0.9783	0.9416	0.7500

N.A indicates not applicable.

Table 4 Performance comparison with the state-of-the-art methods on the STARE dataset

Type	Methods	Year	Se	Sp	Acc	F -measure
supervised methods	Staal <i>et al.</i> [6]	2004	N.A	N.A	0.9516	N.A
	Li <i>et al.</i> [4]	2016	0.7726	0.9844	0.9628	N.A
unsupervised methods	Jiang and Mojon [21]	2003	N.A	N.A	0.9009	N.A
	Martinez-Perez <i>et al.</i> [24]	2007	N.A	N.A	0.9410	N.A
	Yin <i>et al.</i> [17]	2012	0.7249	0.9666	0.9413	N.A
	Li <i>et al.</i> [15]	2012	0.7191	0.9687	0.9407	N.A
	Wang <i>et al.</i> [25]	2015	0.7686	0.9660	0.9451	N.A
	proposed method	2017	0.7126	0.9726	0.9474	0.7332

N.A indicates not applicable.

vessel extraction on the basis of a training set and has an excellent clinic value.

5 Conclusion

We have presented a double-scale thresholding method based on VSRs to segment vessels from retinal images. First, we utilise the DSF method to enhance the contrast between the foreground vascular and the background stuff. Second, we segment the fine and coarse vessels by the proposed ALT and FRT methods, respectively. Third, the final binary segmentation is obtained by FFC vessels. As a result, our method achieves a fine segmentation in comparison with the other state-of-the-art unsupervised methods.

6 Acknowledgments

This work was partly supported by the Fundamental Research Funds for the Central Universities (2014JBZ003, 2016JBZ006), the Beijing Natural Science Foundation (no. J160004), and the Shanghai Research Program (no. 17511102900).

7 References

- [1] Pires, R., Jelinek, H.F., Wainer, J., *et al.*: 'Assessing the need for referral in automatic diabetic retinopathy detection', *IEEE Trans. Biomed. Eng.*, 2013, **60**, (12), pp. 3391–3398
- [2] Welikala, R., Fraz, M., Williamson, T., *et al.*: 'The automated detection of proliferative diabetic retinopathy using dual ensemble classification', *Int. J. Diagnostic Imaging*, 2015, **2**, (2), p. 72
- [3] Zhao, Y., Rada, L., Chen, K., *et al.*: 'Automated vessel segmentation using infinite perimeter active contour model with hybrid region information with application to retinal images', *IEEE Trans. Med. Imaging*, 2015, **34**, (9), pp. 1797–1807
- [4] Li, Q., Feng, B., Xie, L., *et al.*: 'A cross-modality learning approach for vessel segmentation in retinal images', *IEEE Trans. Med. Imaging*, 2016, **35**, (1), pp. 109–118
- [5] Zhu, C., Zou, B., Zhao, R., *et al.*: 'Retinal vessel segmentation in colour fundus images using extreme learning machine', *Comput. Med. Imaging Graph.*, 2017, **55**, pp. 68–77
- [6] Staal, J., Abramoff, M.D., Niemeijer, M., *et al.*: 'Ridge-based vessel segmentation in color images of the retina', *IEEE Trans. Med. Imaging*, 2004, **23**, (4), pp. 501–509
- [7] Soares, J.V., Leandro, J.J., Cesar, R.M., *et al.*: 'Retinal vessel segmentation using the 2-D Gabor wavelet and supervised classification', *IEEE Trans. Med. Imaging*, 2006, **25**, (9), pp. 1214–1222
- [8] Ricci, E., Perfetti, R.: 'Retinal blood vessel segmentation using line operators and support vector classification', *IEEE Trans. Med. Imaging*, 2007, **26**, (10), pp. 1357–1365
- [9] Marin, D., Aquino, A., Gegundez-Arias, M.E., *et al.*: 'A new supervised method for blood vessel segmentation in retinal images by using gray-level and moment invariants-based features', *IEEE Trans. Med. Imaging*, 2011, **30**, (1), pp. 146–158
- [10] Fraz, M.M., Remagnino, P., Hoppe, A., *et al.*: 'An ensemble classification-based approach applied to retinal blood vessel segmentation', *IEEE Trans. Biomed. Eng.*, 2012, **59**, (9), pp. 2538–2548
- [11] Cheng, E., Du, L., Wu, Y., *et al.*: 'Discriminative vessel segmentation in retinal images by fusing context-aware hybrid features', *Mach. Vis. Appl.*, 2014, **25**, (7), pp. 1779–1792
- [12] Chaudhuri, S., Chatterjee, S., Katz, N., *et al.*: 'Detection of blood vessels in retinal images using two-dimensional matched filters', *IEEE Trans. Med. Imaging*, 1989, **8**, (3), pp. 263–269
- [13] Hoover, A., Kouznetsova, V., Goldbaum, M.: 'Locating blood vessels in retinal images by piecewise threshold probing of a matched filter response', *IEEE Trans. Med. Imaging*, 2000, **19**, (3), pp. 203–210
- [14] Zhang, B., Zhang, L., Zhang, L., *et al.*: 'Retinal vessel extraction by matched filter with first-order derivative of Gaussian', *Comput. Biol. Med.*, 2010, **40**, (4), pp. 438–445
- [15] Li, Q., You, J., Zhang, D.: 'Vessel segmentation and width estimation in retinal images using multiscale production of matched filter responses', *Expert Syst. Appl.*, 2012, **39**, (9), pp. 7600–7610
- [16] Zou, P., Chan, P., Rockett, P.: 'A model-based consecutive scanline tracking method for extracting vascular networks from 2-d digital subtraction angiograms', *IEEE Trans. Med. Imaging*, 2009, **28**, (2), pp. 241–249
- [17] Yin, Y., Adel, M., Bourennane, S.: 'Retinal vessel segmentation using a probabilistic tracking method', *Pattern Recognit.*, 2012, **45**, (4), pp. 1235–1244
- [18] Mendonca, A.M., Campilho, A.: 'Segmentation of retinal blood vessels by combining the detection of centerlines and morphological reconstruction', *IEEE Trans. Med. Imaging*, 2006, **25**, (9), pp. 1200–1213
- [19] Nguyen, U.T., Bhuiyan, A., Park, L.A., *et al.*: 'An effective retinal blood vessel segmentation method using multi-scale line detection', *Pattern Recognit.*, 2013, **46**, (3), pp. 703–715
- [20] Wang, Y., Ji, G., Lin, P., *et al.*: 'Retinal vessel segmentation using multiwavelet kernels and multiscale hierarchical decomposition', *Pattern Recognit.*, 2013, **46**, (8), pp. 2117–2133
- [21] Jiang, X., Mojon, D.: 'Adaptive local thresholding by verification-based multithreshold probing with application to vessel detection in retinal images', *IEEE Trans. Pattern Anal. Mach. Intell.*, 2003, **25**, (1), pp. 131–137
- [22] Epshtein, B., Ofek, E., Wexler, Y.: 'Detecting text in natural scenes with stroke width transform'. Proc. IEEE Conf. on Computer Vision & Pattern Recognition, California, USA, 2010, pp. 2963–2970
- [23] Von Gioi, R.G., Jakubowicz, J., Morel, J.M., *et al.*: 'LSD: a fast line segment detector with a false detection control', *IEEE Trans. Pattern Anal. Mach. Intell.*, 2010, **32**, (4), pp. 722–732
- [24] Martinez-Perez, M.E., Hughes, A.D., Thom, S.A., *et al.*: 'Segmentation of blood vessels from red-free and uorescein retinal images', *Med. Image Anal.*, 2007, **11**, (1), pp. 47–61
- [25] Wang, X.H., Zhao, Y.Q., Liao, M., *et al.*: 'Automatic segmentation for retinal vessel based on multi-scale 2D Gabor wavelet', *Acta Autom. Sin.*, 2015, **41**, (5), pp. 970–980